

# Accretion Disk Illumination in Schwarzschild and Kerr Geometries: Fitting Formulae

Keigo Fukumura & Demosthenes Kazanas

*Astrophysics Science Division, NASA Goddard Space Flight Center, Code 663, Greenbelt,  
MD 20771*

fukumura@milkyway.gsfc.nasa.gov, Demos.Kazanas-1@nasa.gov

## ABSTRACT

We describe the methodology and compute the illumination of geometrically thin accretion disks around black holes of arbitrary spin parameter  $a$  exposed to the radiation of a point-like, isotropic source at arbitrary height above the disk on its symmetry axis. We then provide analytic fitting formulae for the illumination as a function of the source height  $h$  and the black hole angular momentum  $a$ . We find that for a source on the disk symmetry axis and  $h/M > 3$ , the main effect of the parameter  $a$  is allowing the disk to extend to smaller radii (approaching  $r/M \rightarrow 1$  as  $a/M \rightarrow 1$ ) and thus allow the illumination of regions of much higher rotational velocity and redshift. We also compute the illumination profiles for anisotropic emission associated with the motion of the source relative to the accretion disk and present the fractions of photons absorbed by the black hole, intercepted by the disk or escaping to infinity for both isotropic and anisotropic emission for  $a/M = 0$  and  $a/M = 0.99$ . As the anisotropy (of a source approaching the disk) increases the illumination profile reduces (approximately) to a single power-law, whose index,  $q$ , because of absorption of the beamed photons by the black hole, saturates to a value no higher than  $q \gtrsim 3$ . Finally, we compute the fluorescence Fe line profiles associated with the specific illumination and compare them among various cases.

*Subject headings:* accretion, accretion disks — black holes physics — neutron stars — stars: individual X-rays: reprocessing

## 1. Introduction

The “standard” geometry of accreting active galactic nuclei (AGNs) (and for that matter also galactic black hole candidates) consists of an optically thick, geometrically thin accretion disk that extends to the radius of the innermost stable circular orbit (ISCO) surrounded by a hot ( $T \sim 10^8 - 10^9$  K), X-ray emitting corona. Coronal X-rays are reprocessed on the surface of the much cooler disk ( $T \sim 10^4 - 10^6$  K) to produce fluorescent Fe  $K\alpha$  emission line at 6.4 keV as well as a reflection component; the latter constitutes a broad peak near  $E \simeq 30$  keV resulting from the reprocessing of the power law coronal emission on the colder disk by reducing its flux by photoelectric absorption at low energies and by down-Comptonization at high energies.

The intrinsically narrow shape and the well known energy (6.4 keV) of the  $K\alpha$  line make it a unique diagnostic of the inner regions of accretion flows around black holes: An accretion disk such as those described above is expected to produce line profiles of unique shapes because of the large Doppler motion and redshifts associated with emission from the innermost radii of such disks (see however Titarchuk et al. 2003, for an alternative view). Model fluorescence  $K\alpha$  profiles have been computed for disks around either Schwarzschild (Fabian et al. 1989) or Kerr (e.g., Laor 1991; Beckwith & Done 2004; Dovčiak, Karas, & Yaqoob 2004; Brenneman & Reynolds 2006) black holes, while more general treatment including the reflection component has also been discussed (e.g., George & Fabian 1991; Matt, Perola, & Piro 1991).

The advent of observation has subsequently vindicated these considerations with the discovery of broad iron  $K\alpha$  lines (e.g., Tanaka et al. 1995; Nandra et al. 1997). Of particular interest has been the  $K\alpha$  line associated with the AGN MCG –6-30-15, which, because of its very broad red wing, indicated emission by matter interior to the radius of the ISCO of a Schwarzschild black hole ( $r/M = 6$  where  $M$  is the black hole mass), thereby implying emission by an accretion disk around a highly rotating Kerr black hole (Iwasawa et al. 1996). Observations of the same object by the much larger area of *XMM-Newton* increased the significance of these observations and confirmed the presence of a very broad line (Wilms et al. 2001; Fabian et al. 2002), however the low sensitivity of the instrument above  $\gtrsim 10$  keV has made difficult the determination of the underlying continuum and therefore the true width of the line. More recently, observations of MCG –6-30-15 by Miniutti et al. (2007) with *Suzaku*, with improved sensitivity at higher energies over *XMM-Newton*, were able to confirm that the Fe  $K\alpha$  line in this object is indeed as broad as it was originally claimed.

Clearly, the profile of the Fe  $K\alpha$  emission depends, besides the geometric properties of the accretion disk, also on its kinematic properties and on its illumination by the X-ray continuum source. While the aforementioned treatments, as well as most of similar treatments in the literature assume axisymmetry and Keplerian motion for the plasma in the disk, these assumptions are not guaranteed by any fundamental principle. Non-axisymmetric

structures and/or non-negligible radial velocity in the disk can yield lines of different shapes as shown by some authors (e.g., Ruszkowski 2000; Yu & Lu 2000; Fukumura & Tsuruta 2004). Finally, even in axisymmetric geometries, different illumination laws can yield line profiles of different shapes, as originally shown by Laor (1991). For computational simplicity, a (broken) power-law form ( $r^{-q}$  where  $q > 0$ ) for the illumination function is generally assumed (e.g., Fabian et al. 2002). Laor (1991) has presented line profiles both with such illumination laws as well as with that of an infinite plane by a point source at height  $h$  in flat space, i.e.,  $F(x) = h/[4\pi(h^2 + x^2)^{3/2}]$ , where  $x$  is the distance on the disk plane from the foot of the vertical line from the source to the plane.

The sensitivity of the line profiles on this parameter (see Laor 1991, Fig. 2) has led us to take a closer look into this issue. This issue has been addressed to a certain extent by Reynolds & Begelman (1997) who computed the illumination for a Schwarzschild black hole assuming an isotropic source at a given height, with emphasis on the contribution to the line emission by matter in free fall region (i.e., plunging region), interior to the ISCO at  $r/M = 6$ . The question we are set to study in this note is the illumination law of an accretion disk by isotropic and non-isotropic point sources at arbitrary values of the height  $h$  and for arbitrary values of the black hole spin parameter  $a$ . Our goal is to produce fitting formulae for the most generic cases which can be easily incorporated into existing numerical/software codes to produce more realistic line profiles for given source configurations. We place some emphasis on the issue of isotropy which changes in the presence of strong gravitational field. We also provide examples of anisotropic illumination by assuming that the source is moving instantaneously and that all anisotropy is due to the relativistic beaming of its photons.

In §2 we outline the setup of the problem and the method followed for the case of a Schwarzschild black hole, while we defer discussion of the Kerr geometry to the Appendix. In §3 we present the results of our calculations along with their fitting formulae in graphic form for comparison with the direct calculation and provide a few examples of the resulting Fe  $K\alpha$  line profiles. Finally in §4 we conclude by summarizing and evaluating our results.

## 2. Formulation of the Problem

We consider an X-ray source located at a height  $h$  above the plane of an accretion disk and along its axis of symmetry as shown in Figure 1. A black hole is located at the origin of the coordinate system, with the accretion disk extending to the ISCO. The latter depends on the spin parameter of the black hole, ranging from  $r/M = 6$  for a Schwarzschild black hole ( $a/M = 0$ ) to  $r/M = 1$  as  $a/M \rightarrow 1$ . We also assume the X-ray emission to be isotropic in the local frame of the X-ray source.

In this part of our treatment we follow the exposition given in Chandrasekhar (1983)



where  $R^2(r) \equiv r^2/(1 - 2M/r)$ .

As shown in Figure 1 we consider photons emitted by the source at (local) polar angles  $\psi$  defined by the expression (see Chandrasekhar 1983, p.127)

$$\cot\psi = \frac{1}{r} \frac{d\tilde{r}}{d\theta} = \frac{1}{r(1 - 2M/r)^{1/2}} \frac{dr}{d\theta}, \quad (5)$$

where  $d\tilde{r} = (1 - 2M/r)^{-1/2}dr$  is the element of proper length in the radial direction and  $r$  and  $\theta$  are the usual Boyer-Lindquist coordinates of the Schwarzschild geometry. We use the above equation (5) for the definition of isotropic photon emission at the local frame of the source, and so we choose their distribution to be uniform in the angle  $\psi$  (i.e., we set  $\Delta\psi = \text{constant}$ ). Using the equation of the photon orbits [equation (4)] and the definition of  $R(r)$ , the above expression for the angle  $\psi$  can be rewritten as

$$\cot^2\psi = \frac{R^2(r)}{b^2} - 1 \quad \text{or} \quad b^2 = R^2(r) \sin^2\psi = \frac{r^2}{(1 - 2M/r)} \sin^2\psi. \quad (6)$$

The above equation (6) provides the necessary relation between the photon impact parameter  $b$  and its local emission angle  $\psi$ .

The photon trajectories of a (locally) isotropic emission are determined by choosing the value of  $\psi$  uniformly between 0 and  $\pi$  and then using equation (6) to determine the value of the photon's impact parameter  $b$  which, substituted in equation (4), provides the associated photon orbits. However, because the photon orbit equation involves the square of the derivative  $dr/d\theta$ , we have found it more convenient to use the second-order equation for  $r$  supplemented with a value for the derivative of the radial coordinate,  $\dot{r}$  ( $\equiv dr/d\tau$ ), to be used as an initial condition. Differentiating equation (1) with respect to  $\tau$  and using equation (6) we obtain the following expressions for the equation of motion and the initial condition on  $\dot{r}$

$$\ddot{r} = \frac{b^2}{r^3} \left(1 - \frac{3M}{r}\right) \quad \text{and} \quad \dot{r}^2 = 1 - \frac{b^2}{R^2(r)} = 1 - \frac{b^2}{r^2} \left(1 - \frac{2M}{r}\right) = \cos^2\psi. \quad (7)$$

Cast in the above form, the photon equation of motion makes apparent the significance of the  $r/M = 3$  surface for photon circular orbits in the Schwarzschild geometry; the second relation then indicates that, because of the single degree of freedom of the photon orbits, the value of  $\dot{r}$  necessary for their specification is uniquely determined by the value of the impact parameter  $b$  or the angle  $\psi$  through this relation.

Our procedure for the determination of the orbits is the following: We consider a large number of orbits determined by the photon emission angle  $\psi$  chosen uniformly between 0 and  $\pi$ . Using equations (6) and (7) we obtain for each value of  $\psi$  the values for  $b$  and  $\dot{r}$  which are used to integrate the second-order photon equation of motion along with that for

the angular momentum,  $d\theta/d\tau = b/r^2$ . The integration proceeds from an initial value  $\theta = 0$  (the location of the source on the symmetry axis) until the angle  $\theta$  reaches the value  $\theta = \pi/2$  (the position of the equatorial plane where the accretion disk lies) at which point we note the value of the radial coordinate  $r$  (now on the surface of the disk) at which the photon is located. Because we launch photons only on the poloidal plane from a source located on the symmetry axis of the source – black hole configuration, in order to take into account the photons emitted in the azimuthal direction, we weigh each photon intercepting the accretion disk by  $\sin\psi$ , the sine of the local polar photon emission angle. We collect all the (weighted) photons arriving at the disk plane (i.e.,  $\theta = \pi/2$ ) at a given radial interval, from the horizon  $r_H$  to  $r/M = 2000$  which is then converted to photons per unit area to produce the disk illumination.

### 3. Results

Following the procedure outlined above for a Schwarzschild black hole and for a Kerr black hole in the Appendix we have produced the illumination of accretion disks for a variety of values for the black hole spin parameter  $a$  and height of the source,  $h$ , expressed in units of the black hole mass  $M$ . Our results along with the fitting formulae appropriate for a most generic case, namely that of an isotropic point source on the symmetry axis, are given in the next subsection (§3.1). The effects of a locally anisotropic emission are discussed in the following subsection (§3.2), while we conclude this section by presenting the line profiles that result from the corresponding model illumination laws (§3.3).

#### 3.1. Illumination by an Isotropic X-ray Source

We first present our results the case of an isotropic source on the axis of symmetry. In Figure 2 we show several of the calculated photon trajectories in the poloidal plane  $(r, \theta)$  for two cases: (a)  $h/M = 100$  and (b)  $h/M = 3$ . In each case the source is isotropic locally and the photons are chosen in constant angular size intervals of size  $\Delta\psi = 8.7 \times 10^{-2}$  radians = 5 deg (corresponding to a total of  $N = 36$  orbits in the figure). Because of the axial symmetry of the problem we only need show the trajectories of the photons emitted over  $0 \leq \psi \leq \pi$ . The value of black hole angular momentum used in both cases is  $a/M = 0.99$ . For an X-ray source at a height much larger than the black hole horizon (i.e.,  $h/M \gg 1$ ) as in case (a), the disk illumination is not very different from that of the Minkowski geometry given above [ $\propto h/(h^2 + r^2)^{3/2}$ ] (see e.g., Fig. 5a, also to be discussed later). On the other hand, as the source approaches the black hole, as in case (b) of Figure 2, the focusing influence of the geometry becomes significant; the light rays bend toward the black hole and enhance considerably the disk illumination in its vicinity; at the

same time, an increasing fraction of the photons are absorbed by the black hole with the fraction approaching unity as the source position approaches the horizon. It should be noted that in case (b) a significant fraction of the photons are also subjected to frame-dragging by the black hole angular momentum; this causes their rotation in the azimuthal direction before reaching the horizon (note the azimuthal trajectories partially seen just outside the horizon denoted by a dark hole). However, because of the axisymmetry of the configuration, the frame-dragging effects that influence only the azimuthal component of the trajectory are ignorable; the illumination depends on the photon trajectories on the poloidal plane.

The main effects of the black hole angular momentum  $a$ , as far as our current considerations go, mainly lie in the reduction of the sizes of the horizon  $r_H$  and, most importantly, that of ISCO, which allows the illumination of regions of the disk with sufficiently large redshift, a necessary condition for producing the very broad Fe lines observed in MCG –6-30-15. While the photon orbits in the poloidal plane can change significantly with increasing  $a$ , the illumination law depends mainly on the height of the source above the disk  $h/M$  and it is largely independent of the value of  $a$  (this is true for  $h/M \gtrsim 3$ ; for smaller values of this parameter, the illumination laws do differ substantially). We have verified the above statement by direct orbit computation: Figure 3 exhibits the illumination profiles of accretion disks around a Schwarzschild (solid) and a Kerr black hole of  $a/M = 0.99$  (dotted curve) respectively by a source at  $h/M = 3$ . Even for such a small height, the illumination patterns are almost identical, except for the fact that a high value of  $a$  allows smaller value of the horizon  $r_H$  and of ISCO. Because of this the illumination profiles obtained for a Kerr black hole are also appropriate for a black hole with any value of  $a$ , provided that the illumination is restricted to the proper value of ISCO.

By computing a sufficiently large number of orbits in a Kerr geometry with  $a/M = 0.99$ , similar to those appearing in Figure 2, and keeping track of their normalization (proportional to  $\sin \psi$ ) we have calculated the radial distribution of the illumination by collecting the photons intercepting the disk plane within a given range in radius. The results for different values of the parameter  $h/M$  are shown in Figure 4; the values of this parameter used are:  $h/M = 100, 50, 30, 10, 6, 5, 4$  and 3. The inner radius is set to  $r_H/M = 1.15$  (for  $a/M = 0.99$ ) and the outer radius is set to  $r_{\text{out}}/M = 1000$ . In all cases, the illumination approaches asymptotically (i.e., for  $r \gg h$ ) the functional form appropriate for Minkowski space [ $\propto h/(r^2 + h^2)^{3/2} \sim r^{-3}$  for  $r \gg h$ ]; this result is not unexpected as the photons that intercept the outer reaches of the disk have been emitted almost horizontally at the source, directions at which the influence of the focusing effects of the black hole are minimal for the values of  $h/M$  considered here. The normalization of the illumination in this regime of the radius  $r$  is very close to that of Minkowski space too except for the case  $h/M = 3$  in which the gravitational effects “pull” the photon trajectories toward the black hole reducing the normalization below its flat space value (see also Fig. 5d to be explained later). At values of  $r \simeq h$  the profile “levels-off” to a slope which approaches that of flat space ( $\propto r^0$ ). The

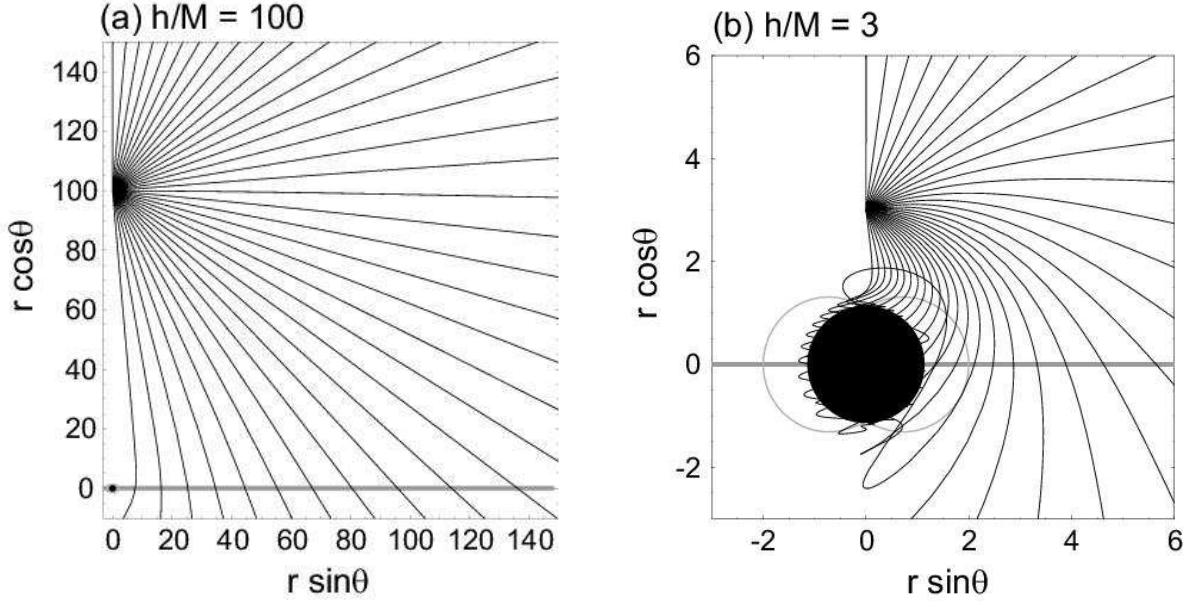


Fig. 2.— Photon trajectories in the poloidal plane  $(r, \theta)$ -plane for (a)  $h/M = 100$  and (b)  $h/M = 3$  around a rotating black hole with  $a/M = 0.99$ . An equatorial thin disk is depicted by the thick gray line at  $\theta = \pi/2$  along with a black hole at  $(0, 0)$ . The gray curve around the black hole denotes the static limit (ergosphere) projected onto this poloidal plane. Scales are different for presentation purposes.

effects of gravitational focusing begin to become noticeable for  $r/M \lesssim 7$  (even for very large values of  $h/M$ ), as shown in Figure 5a; their importance increases with decreasing values of  $h/M$ , as expected and shown in Figure 5a-5d, where the actual illumination is compared to that corresponding to the Minkowski geometry.

The numerical accuracy of our scheme can be assessed by comparing the normalization of the flux of our calculations for large values of  $h/M$  with the analytic result of the flat geometry, which for  $r \ll h$  is  $F_{\text{flat}} \simeq N_{\text{tot}}/(4\pi h^2)$ , where  $N_{\text{tot}}$  is the total number of photons emitted by an isotropic source. Our computation proceeds by launching photons starting at  $\psi = 0$  and incrementing the launch angle by  $\Delta\psi = 5 \times 10^{-5}$  radians. The total number of orbits we compute is then  $N = \pi/\Delta\psi$ ; since each photon is weighted by the sine of the emission angle  $\sin\psi$  (to take into account the number of photons emitted in all azimuths) the corresponding total number of photons emitted by an isotropic source,  $N_{\text{tot}}$ , is related to the number of orbits computed,  $N$ , by the relation

$$N_{\text{tot}} = \sum_{i=0}^N \sin(i\Delta\psi) = \sum_{i=0}^N \sin\left(\frac{i\pi}{N}\right) = \cot\left(\frac{\pi}{2N}\right) \simeq \frac{\pi}{\Delta\psi} \frac{2}{\pi} \quad (\text{for } N \gg 1). \quad (8)$$

Using this value for  $N_{\text{tot}}$  and assuming  $h/M = 100$  (to provide adequate approximation to



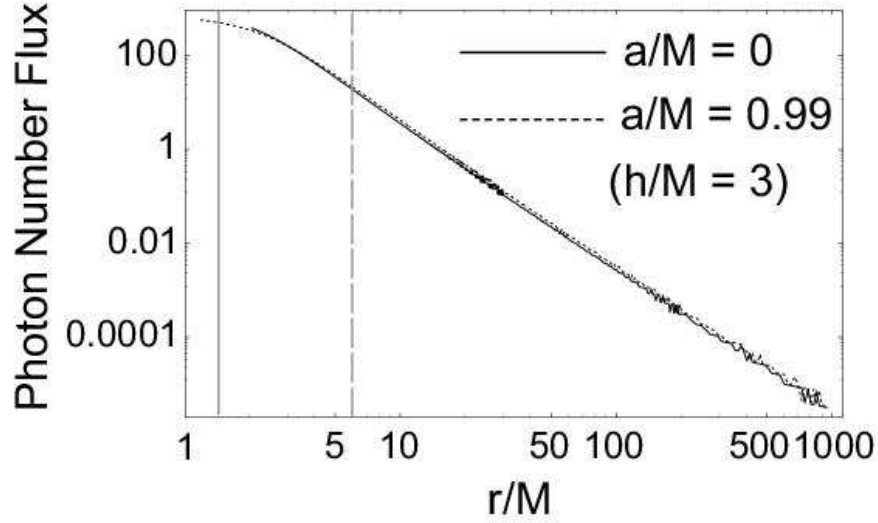


Fig. 3.— Photon number illumination laws as a function of the normalized disk radius  $r/M$  for a Schwarzschild and a Kerr black hole with the values of  $a$  noted in the figure. In both cases the source height has been  $h/M = 3$ . Radius of the ISCO is denoted by vertical dashed line for  $a/M = 0$  and solid line for  $a/M = 0.99$ . The illumination in each case has been computed to  $r = r_H$ .

Minkowski geometry) one obtains for the flux at  $M \ll r \ll h$  (using  $\Delta\psi = 5 \times 10^{-5}$ ) the value  $F_{\text{flat}} = 1/\pi$ , in excellent agreement with the value shown in Figure 4 for the specific value of  $h$ . Our scheme therefore, provides the correct shape and absolute normalization of the illumination at the appropriate limits and we are confident that it provides also the absolute normalization and illumination shape in the regime in which the focusing effects of the geometry are important.

The numerically obtained illumination profiles of Figure 4 were fit with an empirical function of the following form (in the parameter interval noted)

$$F(r, h; K) = K \times \begin{cases} F_1(r, h) & \text{for } 6 < h/M \leq 100, \quad r/M > 1.15 \\ F_2(r, h) & \text{for } 3 \leq h/M \leq 6, \quad r/M > 1.15 \end{cases} \quad (9)$$

where  $K$  is the normalization and the functions  $F_{1,2}(r, h)$  are given by

$$F_1(r, h) = \frac{1.026 \times 10^{-5}(h - 152.9)(h^2 - 158.7h + 6569)}{r^3} - \frac{3.364 \times 10^{-2}(h - 348.7)(h + 11.98)(h + 139.4)}{\{h^2 + (1 + 1/h)^6 r^2\}^{3/2}}, \quad (10)$$

$$F_2(r, h) = \frac{79.56(h - 6.250)(h^2 - 9.763h + 25.19)}{r^3}$$

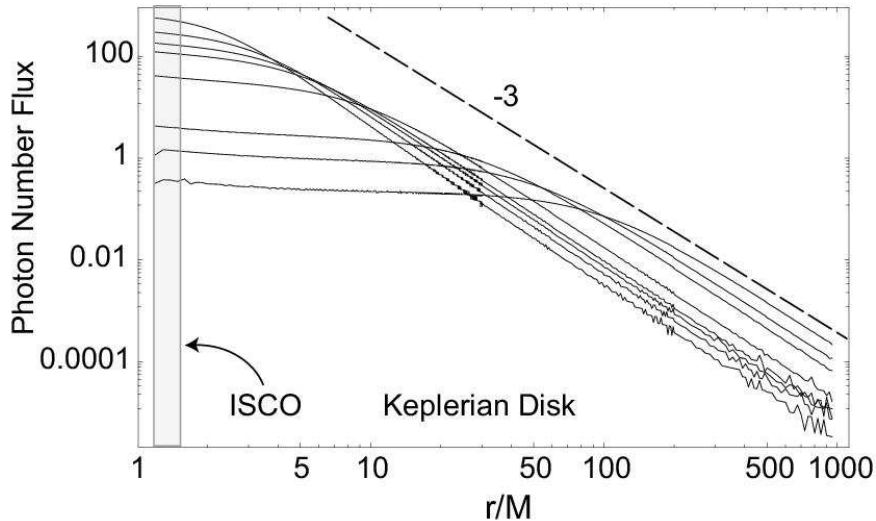


Fig. 4.— Radial illumination profiles of the photon number flux at the disk plane for an isotropic flux of 40,000 photons at the source. We take  $a/M = 0.99$ . The corresponding source heights are  $h/M = 100, 50, 30, 10, 6, 5, 4$  and  $3$ , from bottom to top at the left side of the figure. Dashed line denotes a slope of  $-3$  for power-law form ( $r^{-3}$ ). Plunging region inside ISCO is shown by a shaded box.

$$-\frac{3921(h - 7.364)(h^2 - 8.556h + 21.92)}{\{h^2 + (1 + 1/h)^6 r^2\}^{3/2}}, \quad (11)$$

where  $h$  and  $r$  are measured in units of  $M$ ; the numerical constants that provide the normalization of each of the fractions of the fitting formulae were chosen to give the correct normalization for a total number of photons (by an isotropic source) equal to  $N_{\text{tot}} = 2/\Delta\psi = 40,000$ , i.e. the number appropriate to our own simulations.

In Figure 5 the fits provided by this formula (gray) along with the numerically computed profiles (solid dark) and the corresponding Minkowski geometry profile (dotted curves) are shown for (a)  $h/M = 100$ , (b)  $h/M = 10$ , (c)  $h/M = 6$ , and (d)  $h/M = 3$ . It is apparent that the analytic formulae provide very good fits to the computed curves both in shape and normalization, especially at  $r \lesssim h$ , the region crucial for the correct determination of the relativistic iron line shapes.

It should be noted at this point the above calculations provide the fraction of the total number of photons (number flux) emitted by the source that are intercepted between  $r$  and  $r + dr$  on the disk as measured in Boyer-Lindquist coordinates  $(t, r, \theta, \phi)$  by an observer at rest with respect to the photon source. However, conventional calculations of Fe line profile involve the rate of Fe line photon production as a function of the coordinate  $r$ , measured in the same coordinates by an observer in relative motion with respect to the photon source

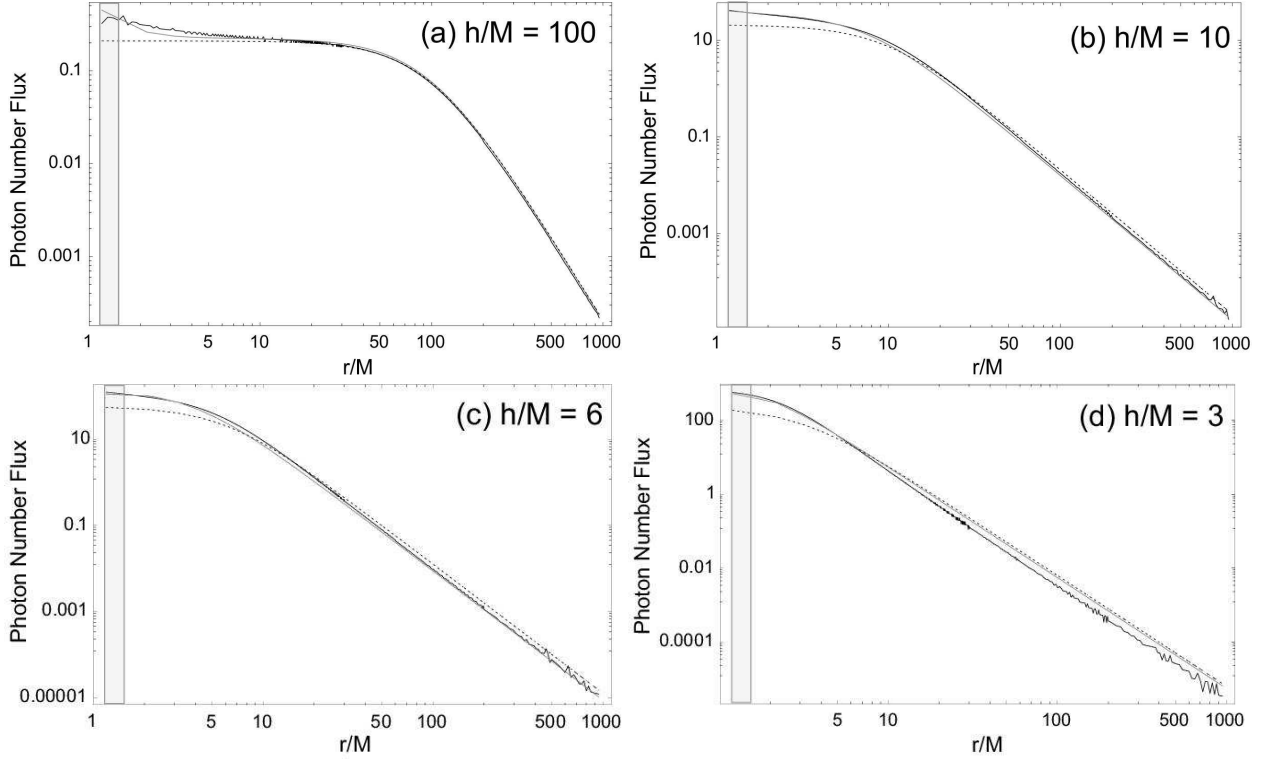


Fig. 5.— The same illumination profiles (solid dark curves) as in Figure 4 for (a)  $h/M=100$ , (b) 10, (c) 6, and (d) 3 along with our best-fitted analytic function (solid gray curves) expressed by equation (9). Dotted curves represent the corresponding profiles in Minkowski space.

with the local Keplerian velocity. Modulo an efficiency factor for the conversion of continuum into line photons, the transformation of the rates between these two Lorentz frames involves powers of the factor

$$\mathcal{D} \equiv \frac{u_r^\mu p_\mu}{u_e^\mu p_\mu}, \quad (12)$$

where  $u_e^\mu$ ,  $u_r^\mu$  are respectively the four-velocities of the emitter and receiver of radiation and  $p_\mu$  the photon four-momenta. The expression of this factor for a source at rest in the Boyer-Lindquist frame and a receiver at rest with the frame moving with the local (disk) Keplerian velocity is computed in Appendix B. The analytic expressions given by equation (9) can be transformed to this frame by multiplying by  $\mathcal{D}^{1+\alpha}$  where  $\alpha$  is the spectral index of the power-law X-ray source (assumed to have the form  $F_\nu \propto \nu^{-\alpha}$  in the local source frame): one power of  $\mathcal{D}$  indicates the change in the rate photons are intercepted by the comoving observer in the fluid/disk frame, while the factor  $\mathcal{D}^\alpha$  accounts for the spectral shift in the photon energy as perceived by the same comoving observer.

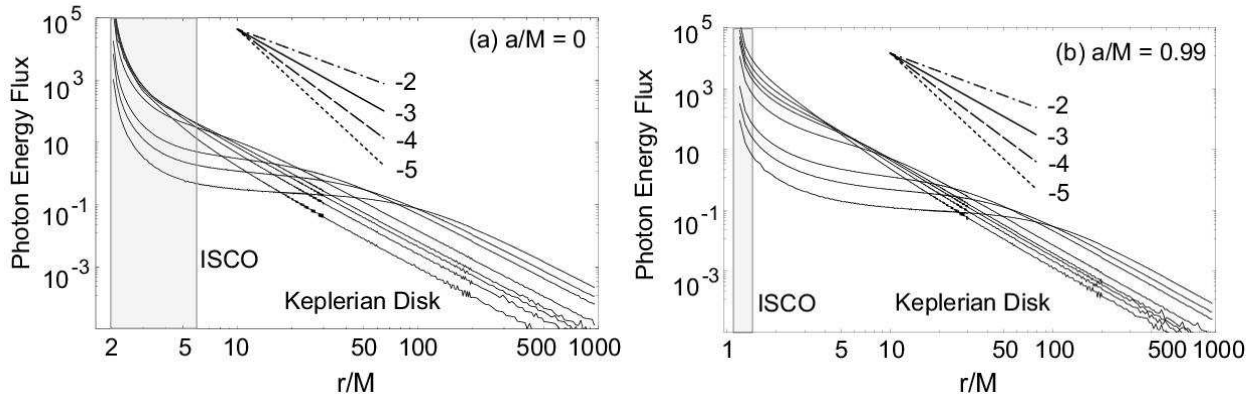


Fig. 6.— Radial illumination profiles, corresponding to Figure 4, of the photon energy flux in the comoving fluid frame. Various slopes are shown as a reference.

In Figure 6 we present the results of this section modified by the above factor (photon energy flux) for a Schwarzschild and a Kerr ( $a/M = 0.99$ ) geometry; i.e.  $F(r, h; K)\mathcal{D}^{1+\alpha}$ . We assume a Keplerian motion outside the ISCO while a free-fall motion in the plunging region. One sees that in both cases there is a considerable increase in the line production rate for sufficiently small radii. Since the slope of illumination in photon energy flux is always steeper than that of the photon number flux by the factor of  $\mathcal{D}^{1+\alpha}$ , the illumination profile of the photon energy flux exhibit two characteristics: the slope of the outer disk zone follows that of flat space ( $q \sim 3$ ), while in the inner disk zone (outside the ISCO) the slope becomes (somewhat) steeper ( $3 \lesssim q \lesssim 4$ ). Inside the ISCO the slope becomes extremely steep simply because of the factor  $\mathcal{D}^{1+\alpha}$ . Assuming that the disks terminate at the ISCO and that there is little emission interior to this radius (as shown in Fig. 3 of Reynolds & Begelman 1997 the matter is expected to be highly ionized in this region, except in cases of very low efficiency), our results indicate that in the case of a Schwarzschild geometry the amplification of the photon flux due to the position and motion of the absorbing plasma on the disk makes only a small change to the results of Figure 4. However, the situation is different in the Kerr geometry examined ( $a/M = 0.99$ ), where the above effect becomes significant at regions of the disk outside the ISCO.

A different aspect of the illumination problem concerns the fraction of the photons of an isotropic source that is intercepted by the accretion disk plane. For a point-like source at height  $h$  on the symmetry axis in Minkowski geometry, the total number of photons intercepted in the region  $r_H < r \leq R$  of the disk is given by

$$N_{\text{flat}} = N_{\text{tot}} \frac{1}{\pi} \left[ \cos^{-1}(h/\sqrt{h^2 + R^2}) - \cos^{-1}(h/\sqrt{h^2 + 1}) \right]. \quad (13)$$

This is the fraction of the total number of photons,  $N_{\text{tot}}$ , emitted within the solid angle subtended by the disk (excluding the black hole horizon, taken in this case to have the value

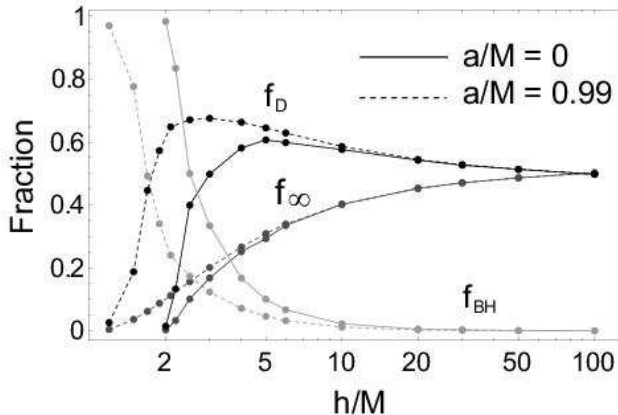


Fig. 7.— The fractions of the photons emitted by an isotropic source that reach the disk plane  $f_D$ , escape to infinity  $f_\infty$ , and lost through the horizon  $f_{BH}$ , as a function of  $h$ . We consider  $a/M = 0$  (solid) and  $a/M = 0.99$  (dotted curves) cases. The cut-off radius is chosen to be  $R/M = 2000$ .

$r_H/M = 1.15 \simeq 1$ ). For  $R \gg h \gg 1$  this attains the value  $N_{\text{tot}}/2$ , the remaining photons escaping to infinity. The focusing effects of the geometry modify significantly the fraction of photons intercepted by the disk, escape to infinity or are absorbed by the black hole as the source approaches the horizon. The procedure we have used in §2 can be used to compute these fractions which are of value in estimating the effects of the geometry on the ratio of line flux to continuum, i.e., the line equivalent width (EW) or the strength of the Compton reflection feature. Figure 7 shows the percentage of the photons of an isotropic source that reach the disk plane (out to a distance  $R/M = 2000$ ),  $f_D$ , that of photons escaping to infinity,  $f_\infty$ , as well as the fraction absorbed by the black hole,  $f_{BH}$ , as a function of the source height  $h$  for  $a/M = 0$  (solid) and  $a/M = 0.99$  (dotted curves). For large  $h$  ( $h/M \gtrsim 50$ )  $f_D, f_\infty \rightarrow 1/2$  while  $f_{BH} \rightarrow 0$ , as expected. As the height of the source decreases,  $f_\infty$  decreases monotonically to zero (for  $h \rightarrow r_H$ ); however,  $f_D$  increases initially reaching a maximum of  $\simeq 70\%$  for  $h/M \simeq 3$  ( $\simeq 60\%$  at  $h/M = 5$  for a Schwarzschild black hole) before it declines to zero as the source approaches the black hole horizon. Last, the fraction  $f_{BH}$  does have the qualitative behavior expected, being negligible for large  $h$ , reaching unity as  $h \rightarrow r_H$ . The qualitative behavior of these quantities does not change as one moves from the case of an extreme Kerr geometry (dotted) to that of a Schwarzschild black hole (solid curves). However, the maximum value of  $f_D$  is slightly smaller and it is achieved for a slightly larger value of  $h$ . It is of interest to note that the values of  $f_{BH}, f_D, f_\infty$  are very similar to those presented by Miniutti et al. (2003), who considered a different source geometry (a ring-like source in an extreme Kerr geometry of radius  $r/M = 2$  located at a height  $h$ ) and a different computational approach. It appears therefore, that this represents a generic behavior for illumination not only by point-like but also by extended X-ray sources provided

that they are concentrated near the symmetry axis of the configuration (rather than, e.g., near the equator).

### 3.2. Illumination by an Anisotropic X-ray Source

While the formulae given above provide very good approximations to disk illumination by an isotropic source, we have chosen to produce also the illumination by an anisotropic emission of photons, appropriate for cases that the observations demand illumination more concentrated near the disk inner edge than that of an isotropic source. Clearly this is an arbitrary choice for if one moves away from the isotropic assumption there is little constraint as to how much anisotropy should be used. Nonetheless, in order to provide an algorithm as well as a gauge of the source anisotropy with a certain theoretical basis we have decided to Lorentz-boost a locally isotropic source distribution along the symmetry axis and toward the black hole by a constant velocity  $v$ . We assume the emission to be instantaneous, i.e., that the photons are emitted before the source has moved substantially to alter its height  $h$ .

The methodology followed is similar to that used earlier: a value of the local angle  $\psi'$  is chosen uniformly as before to provide the photon distribution at the rest frame of the emitter. We then compute the corresponding angle  $\psi$  in the local rest frame which is related to  $\psi'$  by the usual angle transformation

$$\tan\psi = \frac{\sin\psi'}{\gamma(\cos\psi' - \beta)}, \quad (14)$$

where  $\beta \equiv v/c$  and  $\gamma \equiv 1/\sqrt{1 - \beta^2}$ . This value of the angle is then used along with equation (6) to obtain the values of  $b$  and  $\dot{r}$  used in the integration of the photon orbits. The factor  $\sin\psi$  of this latter angle  $\psi$  is again used to provide the correct normalization of the photons illuminating the disk.

As expected, the anisotropy of emission, measured by the velocity of the corresponding relativistic motion, provides a higher concentration of the available photons towards the inner edge of the disk than the geometry alone for a source approaching the disk ( $\beta > 0$ ) and correspondingly less concentrated for a source moving away from the disk ( $\beta < 0$ ). At the same time, depending on the anisotropy and the height of the source, a large fraction of the photons can be lost through the black hole horizon.

Figure 8 shows the photon trajectories by an anisotropic source (moving toward the disk) of anisotropy corresponding to instantaneous velocities (a)  $\beta = 0.5$  and (b)  $\beta = 0.95$  at a height  $h/M = 6$  illuminating a disk around a black hole of  $a/M = 0.99$ . Figure 9 displays the corresponding disk illumination of an anisotropic source for two different values of the source height, namely (a)  $h/M = 6$  and (b)  $h/M = 10$ . For each value of  $h/M$  we consider for comparison source anisotropies corresponding to  $\beta = -0.95, -0.5, 0, 0.5, 0.95$ , with

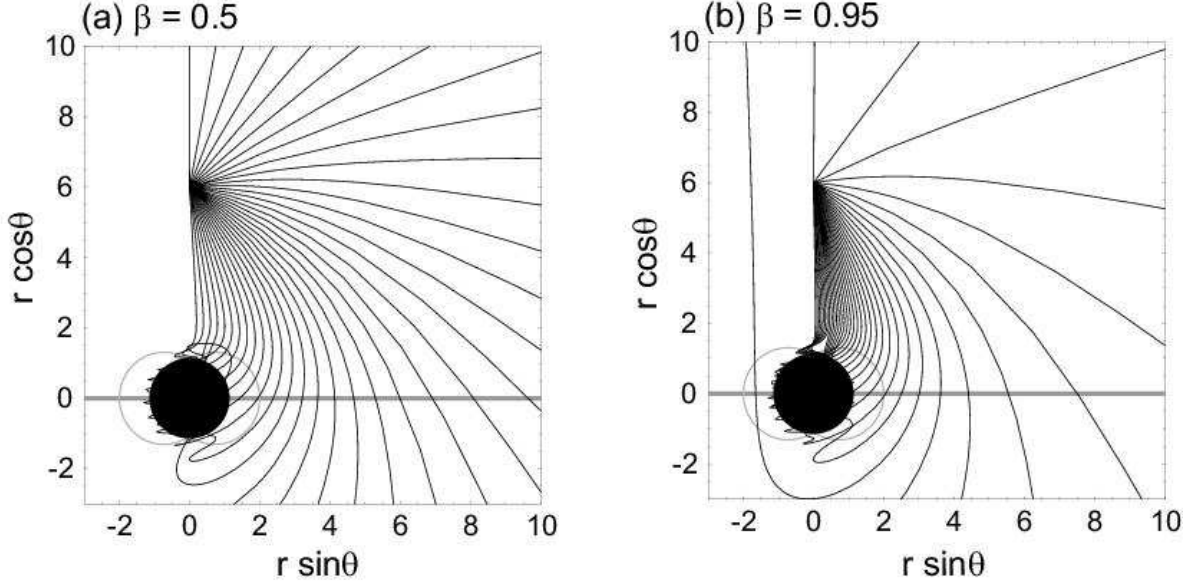


Fig. 8.— The photon trajectories in the poloidal plane for an anisotropic source at  $h/M = 6$  with (a)  $\beta = 0.5$  and (b)  $0.95$ .

the minus sign indicating motion away from the accretion disk. As expected, the anisotropy increases disk illumination for  $r \lesssim h$  for sources approaching the disk, while decreasing it for sources receding from the disk; its slope becomes correspondingly steeper for the higher value of the anisotropy parameter  $\beta = v/c$ . As a result, the profile can deviate greatly from that of an isotropic source. Qualitatively, the increase in  $\beta$  mimics a decrease in  $h$  to the point that  $\cos \psi \simeq 1/\gamma = \sqrt{1 - \beta^2}$ , that is to the point that the Lorentz boosting solid angle ( $\propto 1/\gamma^2$ ) is roughly equal to the solid angle subtended at the source position by the black hole horizon; at this value of  $\beta$  the illumination can be approximated by a power-law  $r^{-3}$  for the entire  $r$ -range as shown in Figure 9; correspondingly a negative value of  $\beta$  (a receding source) provides an illumination profile equivalent to a source at a higher value of  $h$ . We have checked by direct computation that further increase in the anisotropy through an increase in  $\beta$  (or  $\gamma$ ) preserves the  $r^{-3}$  functional form of the illumination (at all distances) but decreases its normalization in proportion to  $\gamma^{-2}$  as might be expected on the basis of qualitative considerations; by contrast increasing of  $|\beta|$  for a receding source, increases indefinitely the effective height of the source  $h$ . Cases that demand an illumination law steeper than  $r^{-3}$  (in number flux) must therefore involve assumptions about the source and its geometry different from those hitherto considered (see §4). On the other hand, energy flux profile can become steeper than  $\sim r^{-3}$  by the factor of  $\mathcal{D}^{1+\alpha}$  in energy flux, as explained earlier. In this respect it is worth considering that a source that could reverse its axial motion ( $\pm\beta$ ) would lead to substantial change in the number of photons intercepting the accretion disk and the flux of the Fe line, even for moderate values of  $|\beta|$  ( $\simeq 0.5$ ).

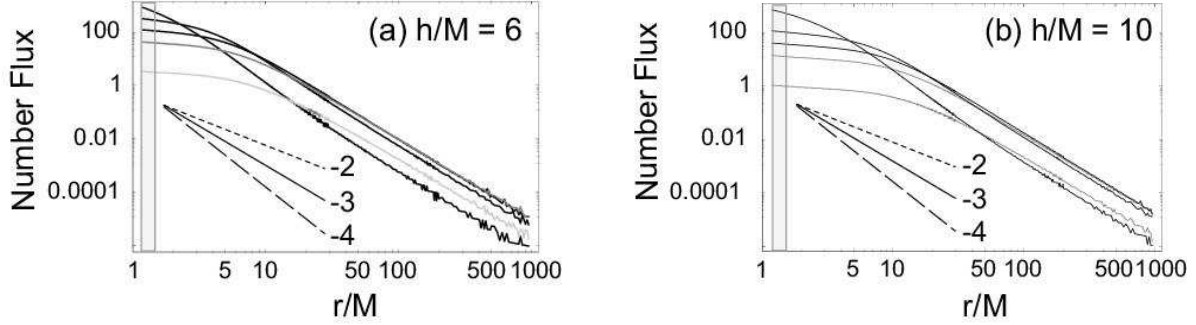


Fig. 9.— The illumination profiles for  $\beta = -0.95$  (gray),  $-0.5$  (gray),  $0, 0.5, 0.95$  from bottom to top at the left side of the figure for (a)  $h/M = 6$  and (b)  $10$ . Three lines represent the slopes for  $-2$  (dotted),  $-3$  (solid) and  $-4$  (dashed lines) as a reference.

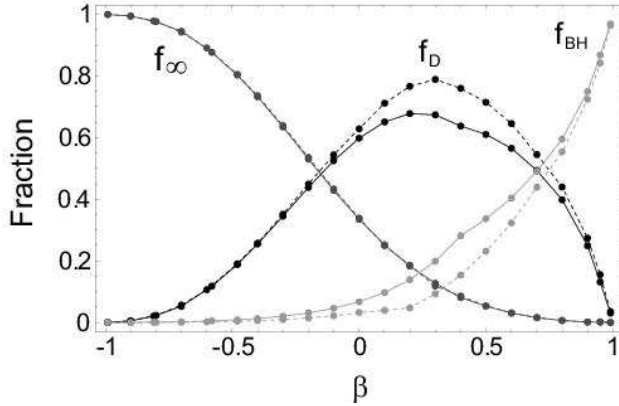


Fig. 10.— Same as Fig. 7 but for anisotropic cases. A source approaching the black hole has  $\beta > 0$ . The source height is set to be  $h/M = 6$ .

For the reasons discussed in the previous subsection we have also computed for the anisotropic illumination case the fractions  $f_{\text{BH}}$ ,  $f_{\text{D}}$ ,  $f_{\infty}$  of the photons intercepted by the black hole, the accretion disk and escaping to infinity, applying the same methodology used in §3.1. These results are shown in Figure 10 for a source at a fixed height  $h/M = 6$  as a function of the anisotropy parameter  $\beta = v/c$  for  $a/M = 0$  (solid) and  $a/M = 0.99$  (dotted curves). For  $\beta = 0$  these fractions are those corresponding to  $h/M = 6$  of Figure 7, as they should. As shown in this figure the maximum (integrated) disk illumination,  $f_{\text{D}}$ , is obtained for  $\beta \simeq 0.3$ . Also as expected,  $f_{\infty}$  decreases with increasing  $\beta$  while  $f_{\text{BH}}$  increases approaching unity as  $\beta \rightarrow 1$ . These fractions are very different from those of flat space, which can be calculated analytically by integrating the appropriate photon angular distribution  $[\propto \gamma^{-2}(1 - \beta\mu)^{-2}]$  over the cosine  $\mu$  of the polar angle  $\theta$  from  $\mu = -1$  to  $\mu = 0$  (for  $f_{\infty}$ ), from  $\mu = 0$  to  $\mu_c = h/\sqrt{1 + h^2}$  (for  $f_{\text{D}}$ ) and from  $\mu_c$  to  $\mu = 1$  (for  $f_{\text{BH}}$ ) where  $\mu_c$  is the cosine of the angle



that the horizon subtends at the distance of the source. In the flat geometry one expects the maximum disk illumination to be obtained for  $\theta \sim 3 \cos^{-1}(\mu_c)$  or  $\beta \simeq \cos[3 \cos^{-1}(\mu_c)] \simeq 0.85$ , a value substantially different from that given in Figure 10, the difference attributed to the focusing effects of the geometry. Also, the ratio of  $f_D$  to  $f_\infty$ , a quantity relevant for the EW of a line, achieves in flat space its maximum value for  $\beta \simeq 0.65$ .

### 3.3. The Iron Line Profiles

In this section we produce the relativistic Fe line profiles corresponding to the illumination laws derived above. The procedure followed for that is the standard ray-tracing method given in the literature (e.g., Fanton et al. 1997; Cadez, Fanton, & Calvani 1998; Beckwith & Done 2004; Fukumura & Tsuruta 2004), by which the photon orbits are followed from the source to the observer’s field of view (or image plane). In all cases the inclination angle of the observer is  $30^\circ$ , relevant for Seyfert 1 galaxies, and the energy resolution is assumed to be  $\Delta E = 150$  eV. We only consider regions outside the ISCO for producing line photons. In Figure 11 sample line spectra are shown for (a) isotropic and (b) anisotropic sources. In (a) the line profiles are shown for  $h/M = 3, 6$  and  $10$  to illustrate the effects of changing the source height on the line profile for  $\beta = 0$ . In (b) we show the line profiles for a source at a fixed height  $h/M = 6$  but of varying anisotropy given by  $\beta = -0.95, -0.5, 0, 0.5$  and  $0.95$  to exhibit the effects of source anisotropy on the corresponding line profiles.

In (a) the profiles are generally broader the closer the source is to the disk due to the increased focusing of the photons toward the disk inner edge. Because the line profiles were produced by collecting photons only out to disk radius  $r_{\text{out}}/M = 30$ , the line flux decreases with decreasing  $h/M$ ; this is because for a decrease in  $h/M$ , the photon flux at  $r/M \gtrsim 10$ , which contributes to the narrow peak of the line near 6.6 keV, decreases, while it increases for the part of the disk that contributes to the low ( $E < 5$  keV) emission. At the same time, however, as shown in Figure 7 the fraction of the photons escaping to infinity also decreases and as a result the line EW will not necessarily decrease (provided that the point source is the only source of illumination).

In (b) the calculated line spectra become broader with increasing anisotropy of an approaching source ( $0 < \beta < 1$ ), simply because more photons are concentrated near the inner edge of the disk. For sufficiently high values of  $\beta > 0$ , the anisotropy beams a large fraction of the photons towards the black hole horizon, resulting in a decrease of the line absolute flux. The red wing of the line, on the other hand, is not suppressed with non-zero flux at energies less than 4 keV. However, as discussed above, the number of photons escaping to infinity (the observer) also decreases and so the EW of the line may not necessarily be negligible. Figure 11b exhibits also, as a reference, the line profile in the same geometry produced by sources receding from the disk ( $\beta < 0$ ). The beaming effect in this case occurs

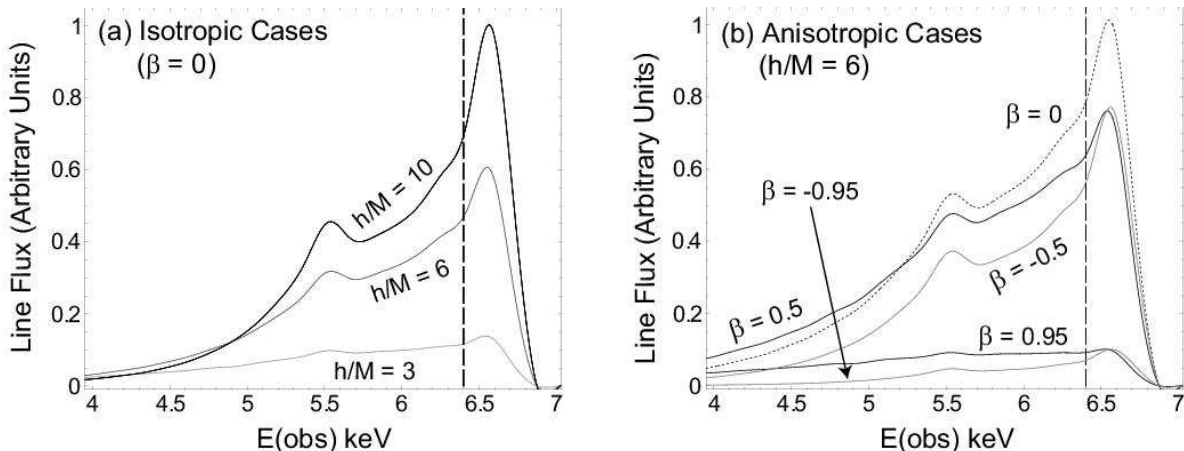


Fig. 11.— Iron line spectra (in arbitrary units) for (a) isotropic and (b) anisotropic sources with  $a/M = 0.99$ . In (a) we show  $h/M = 3, 6$  and  $10$  for  $\beta = 0$  while in (b) we use  $\beta = -0.95, -0.5, 0, 0.5$  and  $0.95$  for  $h/M = 6$ . Vertical dashed line denotes a cold iron line at  $6.4$  keV in the rest frame.

in the opposite direction (away from the black hole) suppressing the overall line flux at all energies.

To provide an estimate of the influence of the source position and anisotropy on the line EW we present in Figure 12 the ratio of the photons escaping to infinity to those intercepting the disk  $f_\infty/f_D$  as a function of (a) the source height  $h/M$  for the case of an isotropic source and (b) the anisotropy parameter  $\beta$  for the case of an anisotropic source at  $h/M = 6$ , i.e. cases that correspond to Figures 7 and 10, respectively. While both fluxes are reduced as the source approaches the black hole (or its anisotropy increases) the ratio of the fluxes intercepted by the disk and escaping to infinity actually increases. All other things remaining equal (e.g. efficiency of Fe line production), this should lead to an increase in the line EW.

#### 4. Discussion & Conclusions

We have produced through direct integration of a large number of photon orbits the illumination law of thin accretion disks around black holes by point-like sources at different heights above the black hole on the axis of symmetry. We have also produced analytic fitting formulae that can provide accurate approximations to the illumination laws (in number flux) under the above assumptions for both Schwarzschild and Kerr black holes. The corresponding energy flux illumination profiles can be obtained by multiplying those by the enhancement factor,  $\mathcal{D}^{1+\alpha}$  appropriate for each situation considered. These can be employed as needed to calculate the corresponding line profiles in a fashion similar to that shown in §3.3. We have

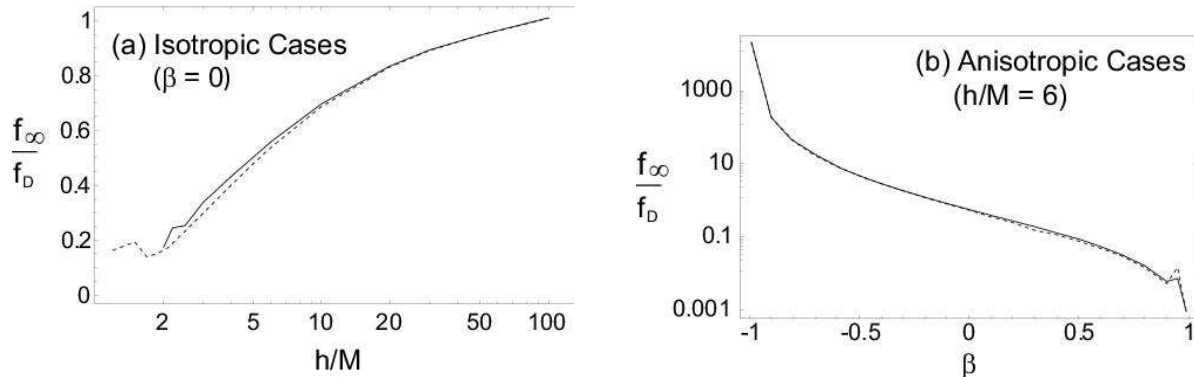


Fig. 12.— The ratio of the fractions of the source photons escaping to infinity to that intercepted by the disk  $f_\infty/f_D$  for (a) an isotropic source (given as a function of the source height  $h/M$ ) and (b) for an anisotropic source (given as a function of the anisotropy velocity  $\beta$ ). Panel (a) corresponds to the flux ratio of Figure 7 while (b) corresponds to the flux ratio of Figure 10. Solid lines are for  $a/M = 0$  while dotted ones for  $a/M = 0.99$ .

also produced for each case the corresponding fractions of photons emitted by the source that escape to infinity, intercept the disk or being absorbed by the black hole, quantities necessary in producing the relative normalization between the escaping (observed) flux and that reprocessed into either the Fe line or the Compton reflection feature. Our overall results can be summarized as follows:

(a) For sufficiently large values of  $h/M$  ( $\gtrsim 50$ ) the illumination profiles of isotropic sources approach those of flat space, with the focusing effects of the geometry becoming noticeable for  $r/M \lesssim 7$ . As the height  $h$  approaches the size of the event horizon, the focusing effects of the geometry concentrates the photon paths to the inner edge of the accretion disk while reducing the illumination of larger radii; these features bear direct relation to the shapes of the resulting line profiles.

(b) In addition to the focusing effects of the geometry, of interest in the production of Fe line photons by the incident radiation is also the increased rate of photon reception and the photon energy shift between the emitting source and the receiving plasma, on a Keplerian orbit on the accretion disk. Assuming that the disk and line production is important only for radii larger than that of ISCO, this amplification is significant for an extreme ( $a/M = 0.99$ ) Kerr geometry but not for a Schwarzschild one. As shown in Figures 4 and 6 the main effect of the hole spin parameter  $a$  is to reduce the size of the horizon and the size of ISCO, which simply determines the minimum radius at which the illumination (and hence the contribution to the line profile) needs to be calculated. This is a rather surprising outcome of our calculations; despite the different topologies of the orbits with increasing black hole spin  $a$  the resulting illumination laws appear to change very little for  $h/M \gtrsim 3$  (however the

profiles become significantly different for smaller values of  $h$ ). As a result the fitting formulae we provide in §3.1 (with the modifications for the rate and photon energy discussed in §3.1) should suffice to produce illumination profiles by isotropic sources for both Schwarzschild and Kerr black holes.

(c) Motivated by the need of illumination more concentrated to the disk inner radius, in order to explain certain particularly broad Fe lines, we have modeled the illumination of disks by point-like anisotropic sources. We modeled the source anisotropy by Lorentz-boosting an isotropic source along the symmetry axis and toward the black hole by a constant velocity  $\beta$ . We found that for sufficiently large values of  $\beta > 0$ , the illumination law (in number flux) assumes the shape of a single power law  $\propto r^{-3}$ , over the entire range of radii. We have also found that further increase in  $\beta$  does not modify this functional form but simply decreases the overall normalization because of absorption of most of the photons by the black hole. While the black hole spin does not affect the illumination profile it does affect the ratio of source photons intercepted by the disk (which can contribute to the line emission) to those that escape to infinity and contribute to the continuum emission, in particular in the case of anisotropic source illumination.

(d) We found that the photon energy flux illumination law, obtained by multiplication of the photon number flux by the factor  $\mathcal{D}^{1+\alpha}$ , can be significantly steeper in the innermost disk region of a Kerr geometry with an index that approach the value  $q \sim 4$  for a small range in radius.

Our calculations indicate that it is hard to obtain disk illumination profiles more concentrated than those discussed above (demanded by certain observations) within the confines of our assumptions. However, modification of these assumptions should easily allow for much steeper profiles. A point-like source on the symmetry axis is an idealization that simplifies the computational task. A point-like source off axis will greatly enhance the illumination in the region immediately underneath its position; this requires a more complicated non-axisymmetric description, not demanded as yet by the observations (but it may in the future). It is also apparent that an extended source can produce arbitrarily steep illumination profiles depending on the assumption of the radial distribution of the X-ray intensity within the source. In the absence of any physically compelling prescription, it is simplest to approximate the illumination as a combination of power-laws: (a) outer illumination  $\propto r^{-3}$  appropriate for large distances; our results indicate this to be a valid assumption for distances much larger than the vertical extent of the source and (b) a steeper one appropriate for the illumination of the inner portions of the disk. While the computation of the resulting illumination is possible under an extended source assumption by extending the procedure described in this note we do not believe that such a model would lead to any significant insights about the physics of these sources.

To this point we have not discussed at all the nature of the illuminating source. Several

proposals have been made in the literature of which we provide an incomplete list: An accretion disk corona (e.g., Haardt & Maraschi 1991), powered either by magnetic fields threading the disk or by magnetic fields threading the black hole (e.g., Li 2002; Reynolds et al. 2004). An alternative is the emission by shocks in the accretion flows that funnels (through magnetic fields) the disk material onto the black hole (e.g., Fukumura, Takahashi, & Tsuruta 2007, for magnetohydrodynamic shocks in accretion). The source can be either stationary or variable, as such shocks were proposed to be unstable and oscillating (see, e.g., Trussoni et al. 1988; Aoki et al. 2004, for discussion of shock stability). Finally, we have not addressed at all the issue of disk ionization, an issue that affects its line producing efficiency (e.g., Nayakshin, Kazanas, & Kallman 2000; Ballantyne, Ross, & Fabian 2001) as they are not related directly to the main thrust of the present work.

Assuming that the plunging region (inside the ISCO) is optically-thin due to very low mass-accretion rate, photons emitted from the source could in principle cross the plunging region. We have followed photon trajectories (from the source to the equatorial plane) and found that certain of them turned around (due to strong light bending) to hit the bottom side of the disk at larger radii and contribute to the illumination there; we found this contribution to the illumination to be unimportant.

We have produced in §3 fitting formulae for the illumination of accretion disks (in photon number flux), which can be easily converted into the photon energy flux needed in the calculations of Fe line profiles. Our models and fits are consistent with the values implied by spectral fits to the Fe lines of most AGNs. Assuming power-law distributions  $\propto r^{-q}$  for emissivity, the values of the index  $q$  obtained for MCG-5-23-13, NGC 4051 and NGC 3516 in recent *Suzaku* observations (Reeves et al. 2006) are  $q \simeq 2 - 3$ ; our models can accommodate easily the lower values of  $q$  while demanding a reasonably high degree of anisotropy for values  $q \gtrsim 3$ . However, the disk illumination under the assumptions considered in this note cannot account for the width of the Fe line profile of MCG -6-30-15 as obtained either by *XMM-Newton* (Wilms et al. 2001; Fabian et al. 2002) or more recently by *Suzaku* (Miniutti et al. 2007) which demand a very steep ( $q \simeq 4.6$ ) illumination of the inner disk section along with a flatter one ( $q \simeq 2.6$ ) at larger radii. As we discussed earlier, the easiest scheme that could accommodate such a profile would be an extended ( $r/M \simeq 2$ ) rather than the point-like source used in our models. An example of such a source has been given in Miniutti et al. (2003), however we believe that other types of extended sources could provide good fits as well. Another possibility has also been proposed that magnetically-induced torque (on the disk) could produce very steep emissivity profiles (e.g., Li 2002). Modeling such sources goes beyond the scope of the present work and maybe undertaken in the future.

We would like to thank the anonymous referee for a number of useful and insightful suggestions. K.F. was supported in part by an appointment to the NASA Postdoctoral Program at the Goddard Space Flight Center, administered by Oak Ridge Associated Uni-

versities through a contract with NASA.

## REFERENCES

- Aoki, S. I., Koide, S., Kudoh, T., Nakayama, K., & Shibata, K. 2004, *ApJ*, 610, 897
- Ballantyne, D. R., Ross, R. R., & Fabian, A. C. 2001, *MNRAS*, 327, 10
- Beckwith, K., & Done, C. 2004, *MNRAS*, 352, 353
- Brenneman, L. W., & Reynolds, C. S. 2006, *ApJ*, 652, 1028
- Cadez, A., Fanton, C., & Calvani, M. 1998, *New Astronomy*, 3, 647
- Chandrasekhar, S. 1983, *The Mathematical Theory of Black Holes* (Oxford: Oxford Univ. Press)
- Dovčiak, M., Karas, V., & Yaqoob, T. 2004, *ApJS*, 153, 205
- Fabian, A. C., Ree, M. J., Stella, L., & White, N. E. 1989, *MNRAS*, 238, 729
- Fabian, A. C., Vaughan, S., Nandra, K., Iwasawa, K., Ballantyne, D. R., Lee, J. C., De Rosa, A., Turner, A., & Young, A. J. 2002, *MNRAS*, 335, L1
- Fanton, C., Calvani, M., de Felice, F., & Cadez, A. 1997, *PASJ*, 49, 159
- Fukumura, K., & Tsuruta, S. 2004, *ApJ*, 613, 700
- Fukumura, K., Takahashi, M., & Tsuruta, S. 2007, *ApJ*, 657, 415
- George, I. M., & Fabian, A. C. 1991, *MNRAS*, 249, 352
- Haardt, F., & Maraschi, L. 1991, *ApJ*, 380, L51
- Iwasawa, K., et al. 1996, *MNRAS*, 282, 1038
- Laor, A. 1991, *ApJ*, 376, 90
- Li, L.-X. 2002, *ApJ*, 567, 463
- Matt, G., Perola, G. C., & Piro, L. 1991, 247, 25
- Miniutti, G., Fabian, A. C., Goyder, R., & Lasenby, A. N. 2003, *MNRAS*, 344, L22
- Miniutti, G., et al. 2007, *PASJ*, 59, S315

- Nandra, K., George, I. M., Mushotzky, R. F., Turner, T. J., & Yaqoob, T. 1997, *ApJ*, 477, 602
- Nayakshin, S., Kazanas, D., & Kallman, T. R. 2000, *ApJ*, 537, 833
- Reeves, J. N., et al. 2006 (astro-ph/0610436)
- Reynolds, C. S., & Begelman, M. C. 1997, *ApJ*, 488, 109
- Reynolds, C. S., Wilms, J., Begelman, M. C., Staubert, R., & Kendziorra, E. 2004, *MNRAS*, 352, 205
- Ruszkowski, M. 2000, *MNRAS*, 315, 1
- Tanaka, Y., et al. 1995, *Nature*, 375, 659
- Titarchuk, L. G., Kazanas, D., & Becker, P. A. 2003, *ApJ*, 598, 411
- Trussoni, E., Ferrari, A., Rosner, R., & Tsinganos, K. 1988, *ApJ*, 325, 417
- Wilms, J., Reynolds, C. S., Begelman, M. C., Reeves, J., Molendi, S., Staubert, R., & Kendziorra, E. 2001, *MNRAS*, 328, L27
- Yu, Q., & Lu, Y. 2000, *MNRAS*, 311, 161

## 5. Appendix A

In the Appendix A we present the orbit equations which we have integrated in producing Figures 2 and 8 in §3. The symmetry of the problem defines an axis which in general is different from the axis connecting the source to the black hole. In this case, in addition to the total angular momentum  $\mathcal{L}$  of the photon with respect to the black hole, there is also its component about the hole’s rotation axis  $L_z$ . Therefore, in this case the photon has two degrees of freedom, i.e. the impact parameters with respect to the black hole  $\eta \equiv \mathcal{L}/E^2$  and the impact parameter with respect to the hole’s rotation axis  $\xi \equiv L_z/E$ .

In this case the equations of motion in the  $r$  and  $\theta$  directions are

$$\dot{r}^2 = \frac{R(r)}{\Sigma^2} \quad \text{and} \quad \dot{\theta}^2 = \frac{\Theta(\theta)}{\Sigma^2}, \quad (15)$$

where  $\Sigma \equiv r^2 + a^2 \cos^2 \theta$  and  $\Delta \equiv r^2 - 2Mr + a^2$ , with  $a$  being the angular momentum per unit mass associated with the Kerr metric, and the functions  $R(r)$  and  $\Theta(\theta)$  are defined by

$$R(r) \equiv [(r^2 + a^2)E - aL_z]^2 - \Delta[\mathcal{L} + (L_z - aE)^2] , \quad (16)$$

$$\Theta(\theta) \equiv \mathcal{L} - (-a^2 E^2 + L_z^2 \operatorname{cosec}^2 \theta) \cos^2 \theta . \quad (17)$$

In analogy with equation (2) these are supplemented by the following equations for  $\dot{t}$  and  $\dot{\phi}$

$$\dot{t} \equiv \frac{dt}{d\tau} = 2 \frac{(r^2 + a^2)[(r^2 + a^2)E - aL_z] + a\Delta L_z - a^2 E \Delta \sin^2 \theta}{\Delta(2r^2 + a^2 + a^2 \cos 2\theta)} , \quad (18)$$

$$\dot{\phi} \equiv \frac{d\phi}{d\tau} = 2 \frac{a[a^2 E - aL_z + E(r^2 - \Delta)] + L_z \Delta \operatorname{cosec}^2 \theta}{\Delta(2r^2 + a^2 + a^2 \cos 2\theta)} . \quad (19)$$

By dividing equations (16) and (17) above by  $E^2$  and re-expressing them in terms of the impact parameters  $\eta$  and  $\xi$  we obtain

$$R(r) = [(r^2 + a^2) - a\xi]^2 - \Delta[\eta + (\xi - a)^2] , \quad (20)$$

$$\Theta(\theta) = \eta - (-a^2 + \xi^2 \operatorname{cosec}^2 \theta) \cos^2 \theta . \quad (21)$$

Specializing to a source located on the axis of symmetry,  $\xi = 0$ ; then the equations of motion and the integrals of motion read respectively as

$$\Sigma^2 \dot{r}^2 = (r^2 + a^2)^2 - \Delta(\eta + a^2) , \quad (22)$$

$$\Sigma^2 \dot{\theta}^2 = \eta + a^2 \cos^2 \theta , \quad (23)$$

and

$$\dot{t} = 2 \frac{(r^2 + a^2)^2 - a^2 \Delta \sin^2 \theta}{\Delta(2r^2 + a^2 + a^2 \cos 2\theta)} , \quad (24)$$

$$\dot{\phi} = 2 \frac{a(a^2 + r^2 - \Delta)}{\Delta(2r^2 + a^2 + a^2 \cos 2\theta)} . \quad (25)$$

The angle between the axis perpendicular to the disk and the direction of photon emission (we call it  $\delta$  instead of  $\psi$  in this case) is given by an expression equivalent to that of equation (5)

$$\cot \delta = \frac{|g_{rr}|^{1/2} \dot{r}}{|g_{\theta\theta}|^{1/2} \dot{\theta}} = \frac{1}{\Delta^{1/2}} \left[ \frac{(r^2 + a^2)^2 - \Delta(\eta + a^2)}{\eta + a^2 \cos^2 \theta} \right]^{1/2} , \quad (26)$$

which can be readily inverted to provide an expression for the impact parameter  $\eta$  in terms of  $\delta$ , namely

$$\eta(\delta, \theta; r, a) = \frac{1}{\Delta} [(r^2 + a^2)^2 - a^2 \Delta(1 + \cos^2 \theta \cot^2 \delta)] \sin^2 \delta , \quad (27)$$



an equation that reduces to equation (6) for  $a = 0$ .

We follow a procedure similar to that of the Schwarzschild case, i.e. we opt for the numerical integration of second-order equations for  $r$  and  $\theta$ . Being emitted from a point along the symmetry axis ( $\xi = 0$ ) the photons still have one degree of freedom namely the impact parameter  $\eta$ . We use equation (27) to relate the local emission angle  $\delta$  to  $\eta$  and equations (22) and (23) to obtain the initial values of  $\dot{r}$  and  $\dot{\theta}$  necessary for the integrations. The integrations proceed again by a choice of the angle  $\delta$  chosen uniformly between 0 and  $\pi$  from ( $r = h, \theta = 0$ ) until  $\theta = \pi/2$  and  $r$  is greater than the black hole horizon corresponding to the specific value of the hole angular momentum  $a$ . For completeness we present below the second-order equations used in the integrations. These are the following:

$$\ddot{r} = \frac{1}{\Sigma^2} \left[ (a^2 \sin 2\theta \dot{\theta} - 2r\dot{r})\dot{r}\Sigma + 2(r^2 + a^2)r - (r - M)(\eta + a^2) \right], \quad (28)$$

and

$$\ddot{\theta} = \frac{1}{2\Sigma^2} \left[ 2(a^2 \sin 2\theta \dot{\theta} - 2r\dot{r})\dot{\theta}\Sigma - a^2 \sin 2\theta \right]. \quad (29)$$

The general case for a photon source off the axis,  $\xi \neq 0$ , is straightforward to obtain using the general form of the equations for  $R(r)$  and  $\Theta(\theta)$ . However, in this case one needs to choose an additional angle in the (local to the source) azimuthal direction which has to be related to  $\xi$  in a similar fashion. In that case the illumination pattern depends also on the azimuthal angle  $\phi$  and the results sufficiently complicated to be presented within this work.

## 6. Appendix B

As emitted photons hit the accretion disk, its local energy and the rate at which they are intercepted by the disk will be relativistically shifted. In order to calculate photon energy flux measured in fluid/disk comoving frame, one must take those effects into account. Photon redshift factor from an emitter's frame to a receiver's frame is defined as

$$\mathcal{D} \equiv \frac{(\mathbf{u} \cdot \mathbf{p})_r}{(\mathbf{u} \cdot \mathbf{p})_e} = \frac{u_r^\mu p_\mu}{u_e^\mu p_\mu}, \quad (30)$$

where “r” and “e” respectively denote the receiver and emitter. For photon's four-momentum, we have  $\mathbf{p} = (-E, \pm E \sqrt{R(r)}/\Delta, \pm \sqrt{\Theta(\theta)}, \xi E)$  where  $E$  is the photon energy in the emitters frame (Chandrasekhar 1983, p.347). For four-velocity we generally assume  $\mathbf{u} = (u^t, u^r, 0, u^\phi)$ . Thus, we obtain

$$\mathcal{D} = \left( \frac{u_r^t}{u_e^t} \right) \frac{(1 - \xi\Omega \mp \sqrt{R(r)}v^r/\Delta)_r}{(1 - \xi\Omega \mp \sqrt{R(r)}v^r/\Delta)_e}, \quad (31)$$

where  $v^r \equiv u^r/u^t$  and  $\Omega \equiv u^\phi/u^t$ . For example, for photons emitted from a stationary on-axis source ( $\xi = 0$ ) reaching the accretion disk (outside ISCO), we find

$$\mathcal{D} = \frac{u_{\text{disk}}^t}{u_{\text{source}}^t} = \left[ \frac{(g_{tt})_{\text{source}}}{(g_{tt} + 2g_{t\phi}\Omega_K + g_{\phi\phi}\Omega_K^2)_{\text{disk}}} \right]^{1/2}, \quad (32)$$

where  $\Omega_K \equiv \sqrt{M}/(a\sqrt{M} + r^{3/2})$  is Keplerian frequency of the disk (Chandrasekhar 1983, p.336).